Biomaterials 180 (2018) 1–11

Contents lists available at ScienceDirect

Biomaterials

journal homepage: www.elsevier.com/locate/biomaterials

# Induced neuro-vascular interactions robustly enhance functional attributes of engineered neural implants

Erez Shor, Uri Merdler, Inbar Brosh, Shy Shoham[**], Shulamit Levenberg[*]

*Department of Biomedical Engineering, Technion IIT, Haifa, Israel*

ARTICLE INFO

*Article history:*
Received 29 March 2018
Received in revised form
23 June 2018
Accepted 1 July 2018
Available online 4 July 2018

*Keywords:*
Tissue engineering
Engineered neural implants
Neuro-vascular interactions
Induced neural activity
Functional neural activity monitoring
Biomaterials

ABSTRACT

Engineered neural implants have a myriad of potential basic science and clinical neural repair applications. Although there are implants that are currently undergoing their first clinical investigations, optimizing their long-term viability and efficacy remain an open challenge. Functional implants with pre-vascularization of various engineered tissues have proven to enhance post-implantation host integration, and well-known synergistic neural-vascular interplays suggest that this strategy could also be promising for neural tissue engineering. Here, we report the development of a novel bio-engineered neuro-vascular co-culture construct, and demonstrate that it exhibits enhanced neurotrophic factor expression, and more complex neuronal morphology. Crucially, by introducing genetically encoded calcium indicators (GECIs) into the co-culture, we are able to monitor functional activity of the neural network, and demonstrate greater activity levels and complexity as a result of the introduction of endothelial cells in the construct. The presence of this enhanced activity could putatively lead to superior integration outcomes. Indeed, leveraging on the ability to monitor the construct's development post-implantation with GECIs, we observe improved integration phenotypes in the spinal cord of mice relative to non-vascularized controls. Our approach provides a new experimental system with functional neural feedback for studying the interplay between vascular and neural development while advancing the optimization of neural implants towards potential clinical applications.



## 1. Introduction

Spontaneous healing or recovery of the central nervous system (CNS) is limited [1]. Pre-clinical experiments showed that cell therapy might induce regeneration and recovery in various neurological diseases [2] such as Alzheimer's disease [3], Parkinson's disease [4], Amyotrophic lateral sclerosis [5] and Huntington's disease [6,7]. Effective cell therapy for spinal cord injury was also attempted by grafting of neural tissue taken from the peripheral nervous system [8], or by directing differentiation of cells from other sources [9]. However, interventions based on grafts taken from the periphery or injection of cells are still largely ineffective, as a result of cell migration, limited cell viability, lack of definitive guidance signals and the secretion of inhibiting factors by the host [10]. Different approaches were proposed for overcoming these challenges, including implants featuring constraints for guiding the elongating axons [11–13] and various stem cell delivery methods producing therapeutic paracrine effects: mesenchymal stem cells [14], neural progenitors [15] olfactory ensheathing cells [16] and pluripotent stem cells [17]. While neural implants are already taking their first steps as clinical treatments [10,18,19], the overall success and the magnitude of the improvement induced by neural implants are still not definitive, and further developments are required to introduce effective implants to induce recovery of damaged neural tissue in the CNS.

Neural tissue engineering, which attempts to artificially produce functional neural tissue, has key advantages compared to plain injection of cells, by preventing cell migration and providing mechanical support and controlled release of supporting substances [20]. Engineered constructs are also used to model diseases [21], assess drug efficacy [22], study mechanisms [23] and explore potential therapies [24]. However, poor integration of engineered implants leading to limited viability was observed in many different types of engineered tissues [25,26]. A powerful strategy for addressing related integration issues is by pre-vascularization of

* Corresponding author.
** Corresponding author.
*E-mail addresses:* shy@technion.ac.il (S. Shoham), shulamit@bm.technion.ac.il (S. Levenberg).

https://doi.org/10.1016/j.biomaterials.2018.07.001
0142-9612/

the engineered constructs. Pre-vascularization provides better viability and improves implant-host integration [26] in various engineered tissues, including skeletal muscle [27,28], cardiac muscle [29,30], pancreatic beta cells [31] and others [32]. Pre-vascularization of engineered neural tissue was previously attempted to model brain microvasculature [33,34], as a potential treatment for stroke [35] and to mimic the blood-brain barrier. However, these studies did not assess any effects on construct integration. Moreover, the effect of the vasculature on the functional activity of the neural tissue was not measured; yet this could be critical parameter for successful neural tissue transplantation. The effect of vascularization on engineered neural constructs is particularly interesting because of the close interplay between vasculature and neural networks [36,37]. Guidance signals from the vasculature, as well as secreted angiogenic factors may modulate the functional attributes and the performance of the transplanted neural tissue [38] and, therefore, help develop implants featuring better performance.

Here we present a detailed design and study of a construct based on a neuro-vascular co-culture (to be referred herein as neuro-vascular construct) implanted into the spinal cord of a mouse model. We evaluated both *in vitro* and *in vivo* how embedding of endothelial properties into the construct affects its morphology, viability, and integration. Using a novel GCaMP assay to gain functional feedback from the construct, we also assess the impact of vascularization on neural activity. By assessing the construct's cellular level functional performance, we show that the neuro-vascular construct exhibits superior characteristics both *in vitro* and *in vivo* and ultimately lead to better integration.

## 2. Materials and methods

### 2.1. PLLA/PLGA scaffold preparation

Porous sponges composed of 50% PLLA and 50% PLGA were fabricated utilizing a particulate leaching technique to achieve pore sizes of 212–600 μm and 93% porosity. Briefly, PLLA (Polysciences) and PLGA (Boehringer Ingelheim) were dissolved 1:1 in chloroform to yield a 5% (w/v) polymer solution; 0.24 ml of this solution was loaded into molds loaded with 0.4 g sodium chloride particles. The solvent was allowed to evaporate overnight, and the sponges were subsequently immersed for 8 h in distilled water (changed every hour) to leach the salt and create an interconnected, porous structure. Final PLLA/PLGA sponges were square 3 mm $\times$ 3 mm, and 1 mm thick. Before use, sponges were soaked overnight in 70% (v/v) ethyl alcohol and then three times with PBS. Previous works have demonstrated the biocompatibility of PLLA/PLGA porous scaffold and estimated its degradation time to be about 6 months.

### 2.2. Cell culture

Human Umbilical Vein Endothelial Cells (HUVECs) (Lonza) were grown in EGM-2 medium supplemented with endothelial cell growth medium BulletKit-2 (EGM-2 BulletKit, Lonza) and harvested for the experiments during passages 4–8.

Neural cells were extracted by removing and dicing cortical tissue from post-natal day 1 (P1) Sprague Dawley rats in cold PBS solution with 20 mM glucose, chemically dissociated neural cells using trypsin (Biological Industries) then mechanically dissociated neural cells (by forcing a few times through a pipette), and filtered the suspension using a 70 μm cell strainer (Biologix). Cells were grown in culture medium (1.8 mL) composed of Minimal Essential Media (MEM, without phenol red, Sigma) containing 17 mM glucose, 100 μl/ml of NU Serum (BD Biosciences), 30 mg/ml of L-Glutamine (Sigma), 1:500 B-27 supplement (Gibco), 50 ng/ml of Nerve Growth Factor (NGF, Alomone labs), 10 ng/ml of Brain-Derived Neurotrophic Factor (BDNF, R&D systems), 25 μg/ml of Insulin (Sigma), and 2 μg/ml of Gentamicin, while directing the bottom structure towards the medium and maintaining the culture under floating during incubation (CO2 perfusion, 37 °C). Half the volume of the culturing media was replaced twice a week.

### 2.3. Construct preparation

Matrigel construct preparation – $1.4 \times 10^6$ neural cells or co-cultures of neural cells and human umbilical vein endothelial cells (HUVEC) marked with red fluorescent protein-(RFP) cells at ratios of 2.5:1 were suspended in 30 μL of Matrigel (Growth factor reduced, BD Biosciences). Construct was later transferred into a 35 mm petri dish filled with culturing medium made of 1:1 mix of HUVEC medium and neural cell medium described above. Half the volume of the culturing media was replaced twice a week.

PLLA/PLGA construct preparation – $2.5 \times 10^5$ neural cells or $3.5 \times 10^5$ co-cultures of neural cells and HUVEC-RFP cells at ratios of 2.5:1 were suspended in 7 μL of fibrin (Sigma, Israel) and seeded onto a 1mmx1mmx600 μm piece of PLLA/PLGA scaffold in a 24 well plate. The construct was incubated for 20 min until the fibrin polymerized. Then the well was filled with culturing medium made of 1:1 mix of HUVEC medium and neural cell medium described above. Half the volume of the culturing media was replaced twice a week.

Cultures were transfected with adeno-associated virus (AAV) 2.1, encoding for the genetic calcium indicator GCaMP6m with medium response kinetics, under the synapsin promoter (Penn Vector Core), to be selectively expressed in neurons. The vector was introduced to the entire cell population, at concentrations ranging from 6.7 to 22.4 GC/ml. The selected vector concentration depended on the desired imaging time point; to gain sufficient expression for calcium imaging at the first days of the culture *in vitro* higher vector concentrations were required in comparison to imaging at later days, when high concentrations resulted in undesired overexpression of the indicator. The whole construct was transfected to minimize the time from neural cell extraction to seeding the culture on the scaffold to maintain the viability and spontaneous activity characteristics of the neurons [39].

### 2.4. Implantation of neural construct and spinal chamber

All animal experiments were done in strict compliance with Technion IACUC approved protocol. C57/BL Mice were anesthetized using Ketamine/Xylazine. The surgical procedure was carried out as described by Farrar et. Al [40] with the following amendments: after attaching the top part of the chamber and before gluing it, hemi transection of the spinal cord is performed at one side of the spinal cord, partiallevering the dorsal ascending tracts at a distance of 0–0.3 mm from the midline to ~0.3 mm depth, at one side, taking care not to cut the contralateral side or the blood vessel in the centerline of the spinal cord. The PLLA/PLGA construct was implanted in the transection site. The glass window was then attached and sealed.

### 2.5. Immunofluorescence

Mice were sacrificed with CO2 as per the approved IACUC protocol and a section from the spinal cord was immediately perfused with PFA 4%. Spinal cords were dissected, embedded in optimal cutting temperature compound (OCT) and sectioned (5 μm) using a cryostat (Leica CM1850, Germany). Subsequently, primary antibodies, diluted in 5% BSA solution, were applied and incubated at 4 °C, overnight: monoclonal rat anti-mouse CD31 (1:200, BD

Pharmingen 550274). Sections were washed three times in PBS for 5 min, before being incubated with the following secondary antibodies: Cy3-conjugated anti-rabbit IgG (1:100, Jackson Immunoresearch laboratory, PA), at room temperature for 30 min. Sections were then rinsed three times in PBS, for 5 min each, and then cleaned for Fluromount-G (Southern Biotechnology) mounting, and covered with cover slips (#1.5) for slide protection. The slides were then imaged using a confocal microscope. Nuclear DNA was stained using 4,6-diamino-2-phenylindole (DAPI) (1:1000, SIGMA, Israel).

### 2.6. Quantitative PCR (qPCR)

Total RNA was extracted from scaffolds using RNeasy Mini Kit (Qiagen Inc., Valencia, CA) in accordance with the manufacturer's protocol. All samples were reverse transcribed to cDNA using the High-Capacity cDNA RT Kit (Applied Biosystems) according to manufacturer's protocol. TaqMan qRT−PCR was performed in triplicate in 96-well reaction plates. Each reaction contained 10 ng of cDNA in 20 μl of reaction mix (TaqMan Gene Expression Master Mix, Applied Biosystems) containing 1 μl of TaqMan Gene Expression Assay (Applied Biosystems). The following TaqMan Gene Expression primers were used: VEGFA (Hs00900055_m1), rat-NGFR (Rn00561634_m1), rat-NTF3 (Rn00579280_m1), and rat-TUBB3 (Rn01431594_m1). Negative controls (without cDNA) were included. Rat-GAPDH was used as the reference gene for relative quantification. The data were collected and analyzed using Data assist v3.1. The relative gene expression data were analyzed using the ΔΔCt method assuming F = 2ΔΔCt. RQ was normalized to mean bTUB expression of each duplicate.

### 2.7. In vivo imaging

All images were taken using a custom 2-photon microscope with excitation laser at 920 nm (Mai-Tai, US). Activity movies were taken by grabbing 128 × 128 pixels at 8 frames/sec.

### 2.8. In vitro imaging

*In vitro* calcium imaging was performed between days 7−14-21 in culture, using a fluorescence microscope (Nikon) equipped with a piezoelectric device (piezosystem jena) capable of moving the objective lens to multiple focal planes. Three planes, separated by 40 μm intervals were captured at 4 frames per second each to allow revisit of each frame (and consequently each neuron) at 4 Hz, in-line with the GCaMP6m decay time. During the imaging sessions, the cultures were maintained in an incubation chamber (34−37 °C), with CO2 perfusion under sterile conditions, thus allowing multiple imaging sessions of each culture [39].

### 2.9. Volumetric morphology analysis

Analysis was done using custom ImageJ commands. Stack of constructs was acquired by confocal microscopy (LSM700, Zeiss, Germany), then further processed by ImageJ. The green channel (neurons) was converted to binary stack of images using iterative thresholding45. Coverage was calculated as the percentage of pixels exceeding threshold. Binary stack underwent 3D skeleton extraction and analysis [41,42] using FIJI plug-ins. The resultant branch numbers, length and volumes were subsequently analyzed using Excel.

### 2.10. Neuronal activity analysis

Processing was done using custom MATLAB code. *In vitro* video sequences were first separated into planes. Cross talk between planes was reduced using nearest neighbor deconvolution (adjacent planes were convolved with Gaussian representing the intra-plane scattering of the construct and subtracted from the analyzed plane). I-vitro video sequencing underwent affine registration to compensate for tissue motion and Kalman filtering to reduce noise. Fluorescence signals F(t) were averaged on areas manually marked by the user on an average image, then normalized according to ΔF/F(t) = [F(t)-F0(t)]/[F0(t)], where F0 is each cell's 5th percentile fluorescence calculated using a 25-s moving window to remove slow baseline variations. An activity event *in vitro* was detected when the fluorescence F(t) crossed a 50% of the maximum ΔF/F threshold and a network burst was detected when 50% or more of the cells were active in the same time point. Bursts per minute were calculated as the inverse of a three-sample moving average of the time between recorded bursts. *In vivo* activity identification was done by spike detection using a statistical method [43]. Single frame presentation filled each manually marked cell with its average ΔF/F value, overlaid over the average intensity image.

### 2.11. Statistical analysis

Results were expressed as mean ± SEM. All analyses were performed using MATLAB/Excel. Differences between two groups were statistically analyzed by a two-sided T test, except for qPCR where single sided *t*-test was performed. For the *in vivo* construct transplantation experiment, positive activity identification assumed signal intensity exceeded baseline + 5σ of noise level. Significance levels: $^{*}p < 0.05$, $^{**}p < 0.01$, $^{***}p < 0.001$.

## 3. Results

### 3.1. The interplay between neural networks and endothelial cells yields more complex neuronal morphology in vitro

To study the properties of neuro-vascular implants we co-cultured neurons and glia cells extracted from rat P1 cortices with red fluorescent protein (RFP)-marked human-vascular-endothelial cells (HUVEC). We investigated two types of constructs: a Matrigel construct seeded with the co-culture, and another construct where fibrin-suspended co-cultures were seeded on poly-*l*-lactic/poly-*l*-glycolic acid (PLLA/PLGA) scaffolds (the latter being more compatible with transplantation and potential clinical translation [44]). Control constructs were prepared in the same manner, but without endothelial cells. After two days the constructs were transfected with GCaMP6m AAV vectors [45] (Fig. 1A). After 14 days *in vitro* the neuro-vascular Matrigel constructs exhibited qualitatively more complex morphology than the non-vascularized ones, with more elongated axons and interconnections (Fig. 1B). The axons were observed elongating parallel to newly-generated endothelial vasculature (Fig. 1B, right panel). Similarly, PLLA/PLGA constructs containing neural tissue with endothelial cells yielded more complex morphology and more elongated axons compared to the neural-only constructs where we observed the appearance of clusters of neurons, where cells were grouped together without elongating axons (Fig. 1C). However, in contrast to the Matrigel constructs, tubular pre-vascular structures were not observed in these constructs.

Cultures made with brain microvascular endothelial cells instead of HUVEC yielded comparable qualitative morphological results (Supplementary Fig. S1). As calibration and tuning of additional culture was beyond the scope of this project, we focused in studying the interplay between HUVEC- based endothelial and neural networks. Conversely, in co-cultures of fibroblasts and neurons the fibroblasts suppressed most of the neural network due

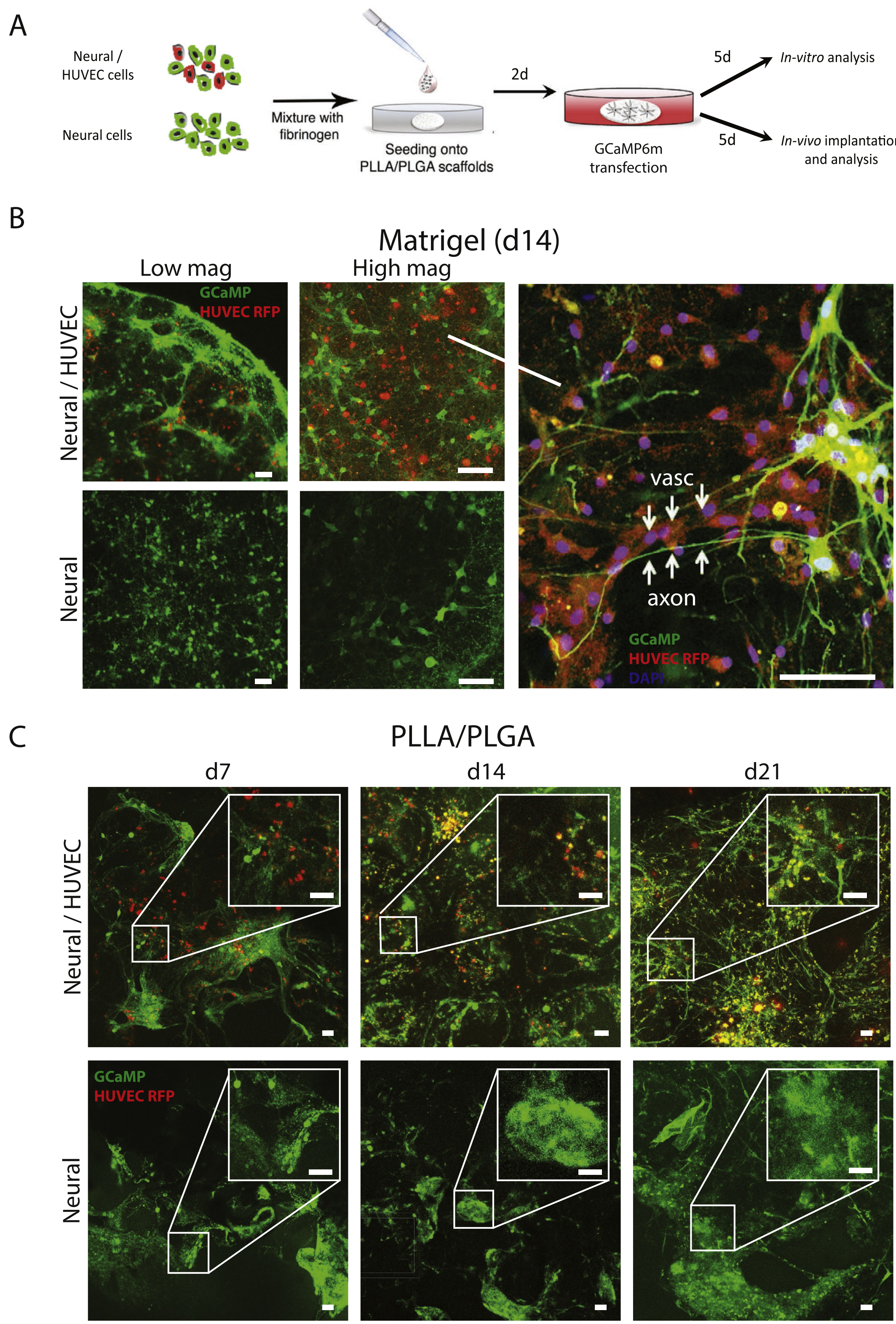


**Fig. 1. Preparation and properties of neuro-vascular and non-vascularized constructs.** (A) Preparation of constructs. (B) Neuro-vascular Matrigel construct at day 14 (top) Vs. non-vascularized construct at day 14 (bottom). Scale bar = 100 µm. (C) Neuro-vascular PLLA/PLGA construct at days 7, 14 and 21 (top) vs. non-vascularized PLLA/PLGA constructs (bottom). Scale bar = 100 µm.

to over-proliferation (Supplementary Fig. S2), rendering this culture unusable for enhancement of neural constructs.

Although matrigel constructs showed more developed tubular pre-vascular structures, they are overall more challenging to use clinically. Once the experimental setup was set up we used PLLA/PLGA scaffolds only for the functional evaluation described below to gain clinical relevance.

To quantify the time-dependent differences between the neuro-vascular and neural PLLA/PLGA constructs we characterized the morphology of the neural and the neuro-vascular constructs using volumetric image processing methods. By reconstructing the 3D features of the neuronal network (Supplementary video 1) we calculated its areal percent coverage, while in the extracted axonal skeleton we identified branching points and axon sections connecting those points. (Fig. 2A).

Supplementary video related to this article can be found at https://doi.org/10.1016/j.biomaterials.2018.07.001.

Neuronal network coverage area expanded over time in both constructs, and from day 7 on was significantly higher ($p < 0.05$) in the neuro-vascular than in the control constructs: while the average coverage of the neuro-vascular constructs increased (13.0% at day 7, 19.0% at day 14 and 23.3% at day 21), the coverage of control constructs plateaued (7.9% at day 7, 11.4% at day 14 and 10.5% at day 21). On the other hand, the control neural constructs developed clusters, which were rarely observed in the neuro-vascular constructs. Both the overall number of branches (defined as axonal segments between defined branching points) and the average length of the longest axon section found in each construct were larger ($p < 0.05$) for the neuro-vascular constructs: while the neuro-vascular cultures had 4279/24546/21035 branches and 0.54/1.62/0.58 mm maximal axonal lengths at days 7, 14 and 21 respectively, the neural constructs exhibited lower values of 1163/13719/8005 branches and maximal axonal lengths of 0.32/0.70/0.14 mm at the respective dates. (Fig. 2B). Finally, to test for co-localization between the neural network and the endothelial cells we calculated the radial cross-correlation function between the images of the neuronal network (green channel, neurons expressing GCaMP6m) and the endothelial cells (red channel, HUVEC cells expressing RFP). The cross correlation peaked at a distance of $47.1 \pm 4.0\ \mu m$ for all time points (Fig. 2C). This peak is indicative of non-random co-localization, in contrast to, perfect (left panel, 'Auto correlation'), or randomly co-localization distributions. (See Supplementary Fig. S3 and S4 for further analysis of radial cross-correlation).

To characterize the expression of neurotrophic factors we performed a qPCR analysis on the neuro-vascular and control constructs. Comparing the abundance of nerve growth factor receptor (NGFR) and neurotrophin3 (NTF3) expressed by the endothelial-neural cultures vs. the neural culture by the qPCR assay, shows that chemical cues inducing neurogenesis and axonal elongation were up-regulated in the neuro-vascular constructs vs. the control: expression of NGFR was 1.5-fold higher and NTF3 expression was 5.2-fold higher (statistically significant differences in both cases, $P < 0.05$, Fig. 2D). To verify we measure only neuronal induced expression of NGFR and NTF3 and we used human specific primers for VEGF as a control, and rat specific primers for NGFR and NTF3.

### 3.2. *Neuro-vascular constructs exhibit enriched activity patterns in vitro*

To characterize the spontaneous neuronal activity in the constructs we virally transfected them with the calcium activity indicator GCaMP6m targeting neurons specifically [46], and on days 14 and 28 performed extended functional imaging of constructs held in a heated chamber [39] (Supplementary video 2). Both the neuro-vascular and the control constructs exhibited spontaneous activity in both time-points (Fig. 3A), with increasingly longer episodes (indicated by wider spikes, Fig. 3B). The observed activity patterns were qualitatively and quantitatively different between the two constructs, with much stronger network bursting activity appearing in the neuro-vascular constructs (Fig 3C; 0.11 vs. 0.7 bursts per 100s for the neural and neuro-vascular, respectively, in day 14, and 0.1 vs. 2.0 in day 28, $p < 0.02$ and $p < 0.014$). In contrast, sporadic activity differences were statistically insignificant (Fig 3C; 14.3 vs. 5.8 events/100s for the neural and neuro-vascular, respectively, in day 14, and 24.1 vs. 24.7 in day 28, $p > 0.6$ using two-sided t-tests). Finally, testing for the generality of the endothelial cell-mediated activity modulation, we observed a similar effect exhibited in the Matrigel constructs, rendering the activity patterns more complex in the neuro-vascular constructs (Supplementary Fig. S5). Unlike the bursatile nature of the neural culture activity, the neuro-vascular culture exhibited more complex activity patterns that combined both network bursts and sporadic activity, indicative of further development of the maturing neuronal culture [39].

Supplementary video related to this article can be found at https://doi.org/10.1016/j.biomaterials.2018.07.001.

### 3.3. *Complex morphology and boosted activity characteristics of the endothelial-neural scaffolds are retained in vivo*

To investigate the *in vivo* cellular processes exhibited by the neuro-vascular construct when implanted in the CNS, we developed a surgical procedure utilizing a mouse spinal dorsal window [40] enabling 2-photon investigation of the spinal cord. We implanted the construct at T10, performing laminectomy and hemi transection under the window chamber to minimize the damage to the spinal cord of the host animals (Fig. 4A). Performing hemi-transection also allowed to partially severe only the dorsal sensory ascending tract on one side, and consequently maintained the animals un-paralyzed, minimizing autophagy and weight loss (Supplementary video 3). Seven days after implantation we inspected the morphological properties of the neuronal network developed. Neuro-vascular constructs appeared to have elongated axons spreading over a larger area compared to the neurons in the control constructs. Clusters were also observed in the control constructs following ex-vivo whole mount analysis of the extracted non-vascularized implant (Fig. 4B). We also noticed the HUVEC RFP cells were maintained in the neuro-vascular constructs (Fig. 4B). Morphology analysis quantified the results and showed wider neuronal coverage in the neuro-vascular constructs compared to the coverage found in the control constructs (Neuro-vascular coverage of 13.6% vs. 5.8% in the neural constructs, $P < 0.006$). The neuro-vascular constructs also exhibited more complicated axonal structure, with longer axons overall and longer axonal sections, partially as a result of the lack of clusters (Branch length of $62.7\ \mu m$ for neuro-vascular vs. $18.2\ \mu m$ for neural constructs, $P < 0.0011$, and total axonal length of 4.0 mm vs. 2.4 mm, $P < 0.04$); the average number of branching points was also larger in the neuro-vascular constructs, but the difference was not statistically significant ($P < 0.1$) (Fig. 4C).

Supplementary video related to this article can be found at https://doi.org/10.1016/j.biomaterials.2018.07.001.

Activity analysis of both types of constructs was done by 2-photon acquisition of high frame rate video sequences. Activity patterns observed in the neuro-vascular constructs were more complex, exhibiting more active cells and a higher average activity rate (Fig. 5B). Statistical analysis of the activity patterns showed that the active fraction of the identified cell population was larger in the neuro-vascular constructs compared to the neural constructs (23.7% were active in the neuro-vascular vs. 5.9% in the neural

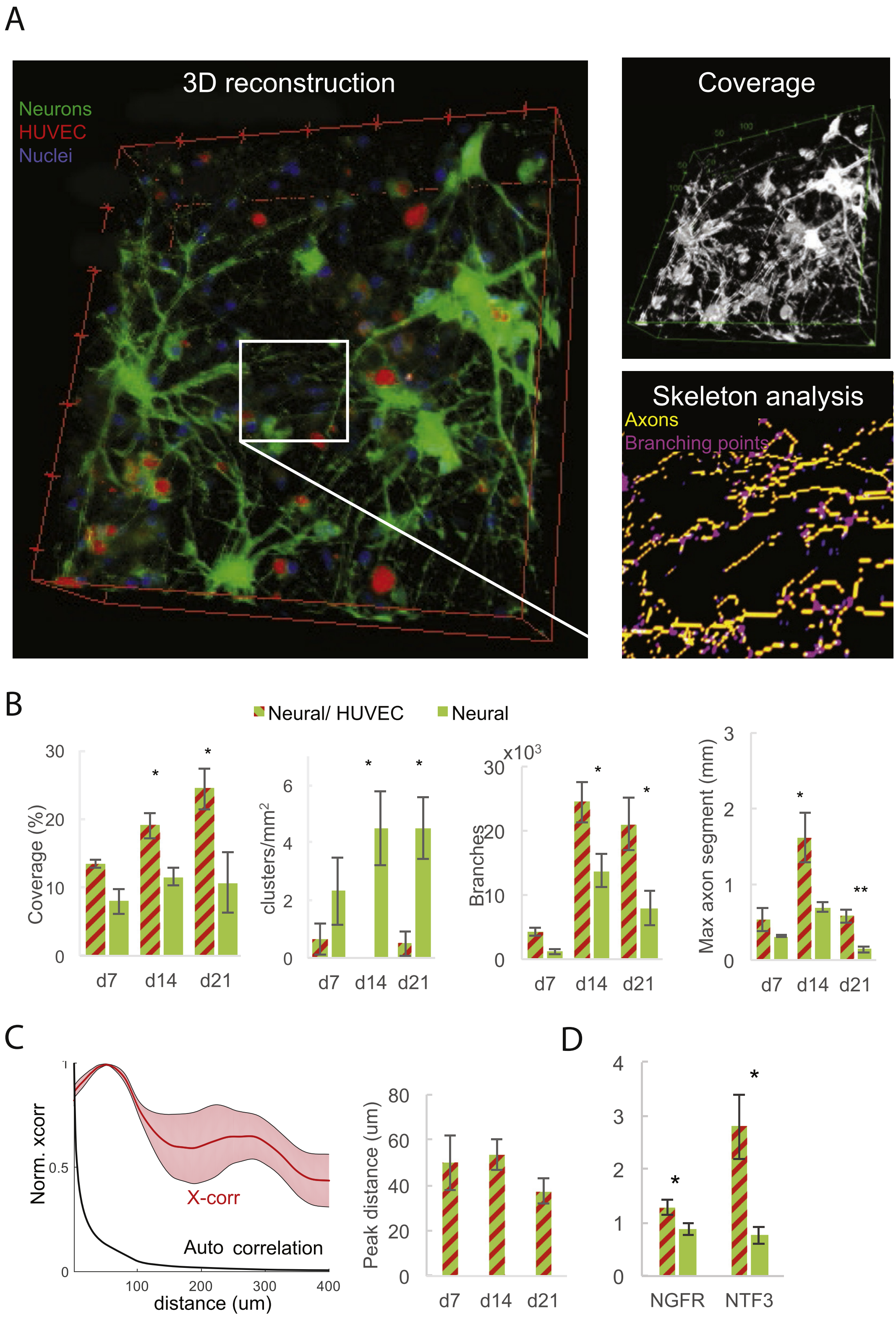


**Fig. 2. Neuro-vascular constructs exhibit more complex morphology.** (A) 3D reconstruction of a neuro-vascular Matrigel constructs based on confocal acquisition of 34 planes(left), Binarization of the neuronal network (green) was projected to calculate coverage (top right), skeleton analysis showing axon sections in yellow and branching points in magenta (top left). Scale bar = 100 µm. (B) Quantification of PLLA/PLGA neuro-vascular vs. non-vascularized morphological properties (left to right): coverage, clusters/mm2, number of branches, maximum axonal length measured. Neuro-vascular constructs n = 11, non-vascularized constructs n = 9. (C) Cross correlation analysis of co-localization. Left-Peak co-localization in radial cross correlation average is at 47.1 µm in neuro-vascular constructs at day 14 (n = 3) vs. peak at zero for auto correlation of neuronal network representing two networks completely aligned. Pink shade represents ± SEM Right-. Peak distance is constant as a function of the age of the construct. n = 9. (D) qPCR results of expression of NGFR and NTF3 in neuro-vascular vs. neural constructs. n = 5. (For interpretation of the references to colour in this figure legend, the reader is referred to the Web version of this article.)

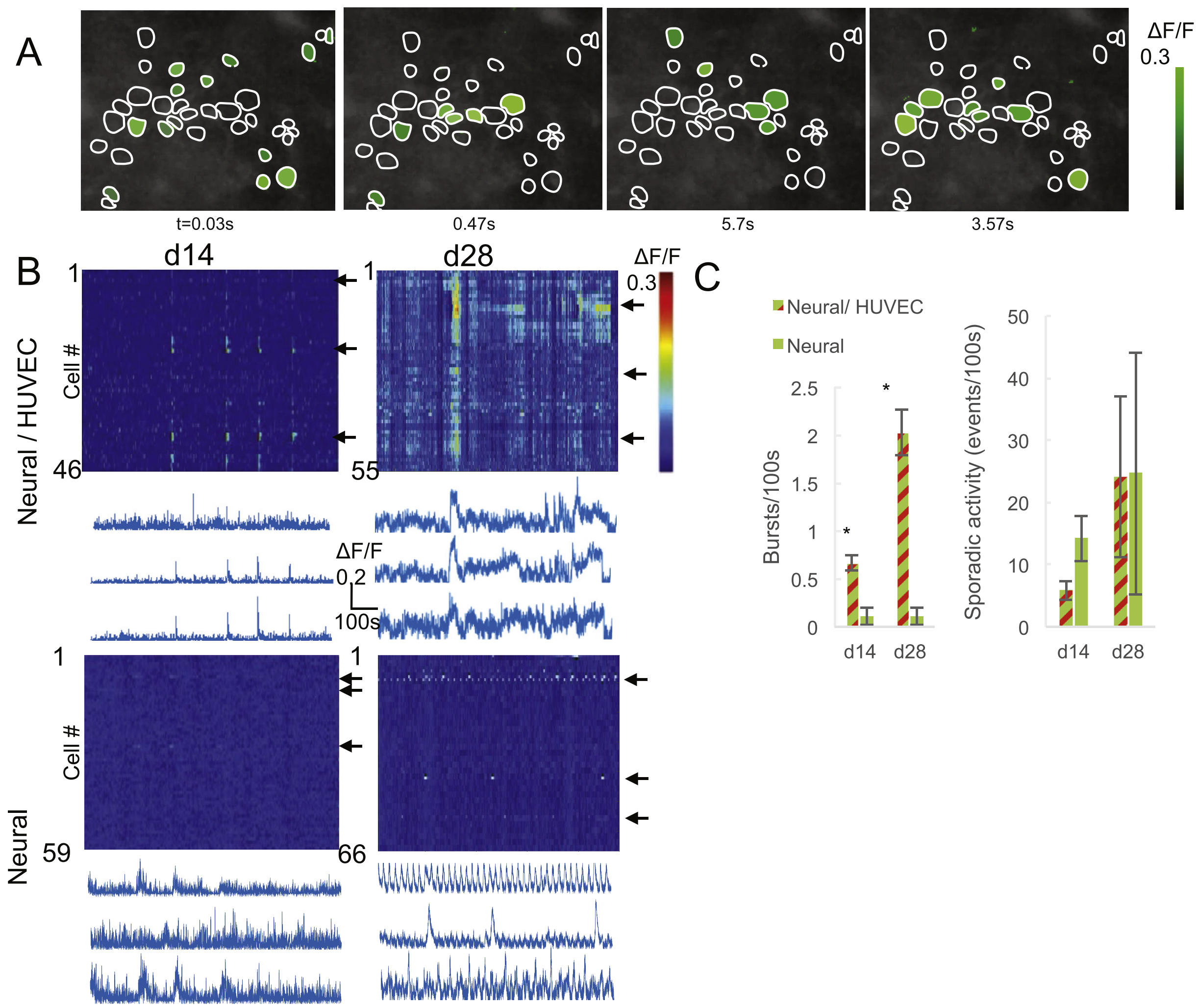


**Fig. 3. Enhanced *in vitro* activity properties of neuro-vascular vs. non-vascularized constructs.** (A) Representative epi-fluorescent neuro-vascular construct images of ΔF/F overlaid on average intensity image showing different neurons active at different time points. Scale bar = 30 μm. (B Representative activity maps and representative ΔF/F temporal signals of neuro-vascular (top) vs. non-vascularized constructs (bottom) at day 14 (left) vs. day 21 (right). (C) Activity analysis of neuro-vascular vs. non-vascularized construct characterizing bursting rate (left) and sporadic activity (right) at days 14 and 21. Neuro-vascular constructs n = 379 cells, 6 constructs. Non-vascularized constructs n = 362 cells, 6 constructs.

culture). We also observed significantly higher overall activity presented by neurons in the neuro-vascular constructs, manifested both in a higher event rate and wider duty cycle (0.2 events/100s overall in the neuro-vascular constructs vs. 0.03 events/100s in the neural constructs, $P < 0.04$). Analysis of the most active cell in each construct showed clearer distinction between the neuro-vascular vs. neural constructs: in the neuro-vascular constructs the ON time was longer (1.54% vs. 0.14%, $P < 0.01$) and the average activity rate higher (10.6 vs. 0.43 events/100s, $P < 0.02$) (Fig. 5C).

### 3.4. Endothelial-neural constructs exhibit better integration properties in vivo

To test the integration of the construct to the host animal we investigated the penetration of host vasculature into the construct 7 days post implantation. Penetration of the host's vasculature into the scaffold was assessed by cryo-sectioning and staining with mouse specific CD31 antigens, which mark endothelial cells. Host vasculature appears denser and more robust in the neuro-vascular constructs (Fig. 6A). Comparing between the vasculature formed in the different constructs reveals a qualitative trend towards more developed vascularization in the neuro-vascular constructs (Fig. 6A). In both cases, the neurons on the implanted construct were not as organized as the axons in the intact spinal cord. However, clusters were still present in the neural constructs, indicating that morphology that is generated during the in-vitro stage is retained (Fig. 6B).

Next, we quantitatively characterized these qualitative vasculature observations by analyzing the morphology of the CD31-stained vasculature that penetrated the construct. The area covered by vasculature was significantly higher for neuro-vascular constructs (5.9% in the neuro-vascular vs. 3.6% in the neural construct, $P < 0.03$), and an additional set of morphological features indicating increased vascular network complexity were also significantly different in the neuro-vascular vs. the neural constructs, respectively (Fig. 6C): vessel length measured in a 1 $mm^2$ area (2.4 mm vs. 1.2 mm, $p < 0.005$), average vessel branch length (17.2 μm vs. 29.6 μm, $p < 0.006$), and total branch points (457 vs. 146, $P < 0.00003$). The longer total vessel length per area indicates the overall coverage of the neuro-vascular constructs is wider. Longer branches with lower number of bifurcations (branch points) observed in the neural constructs compared to shorter branches

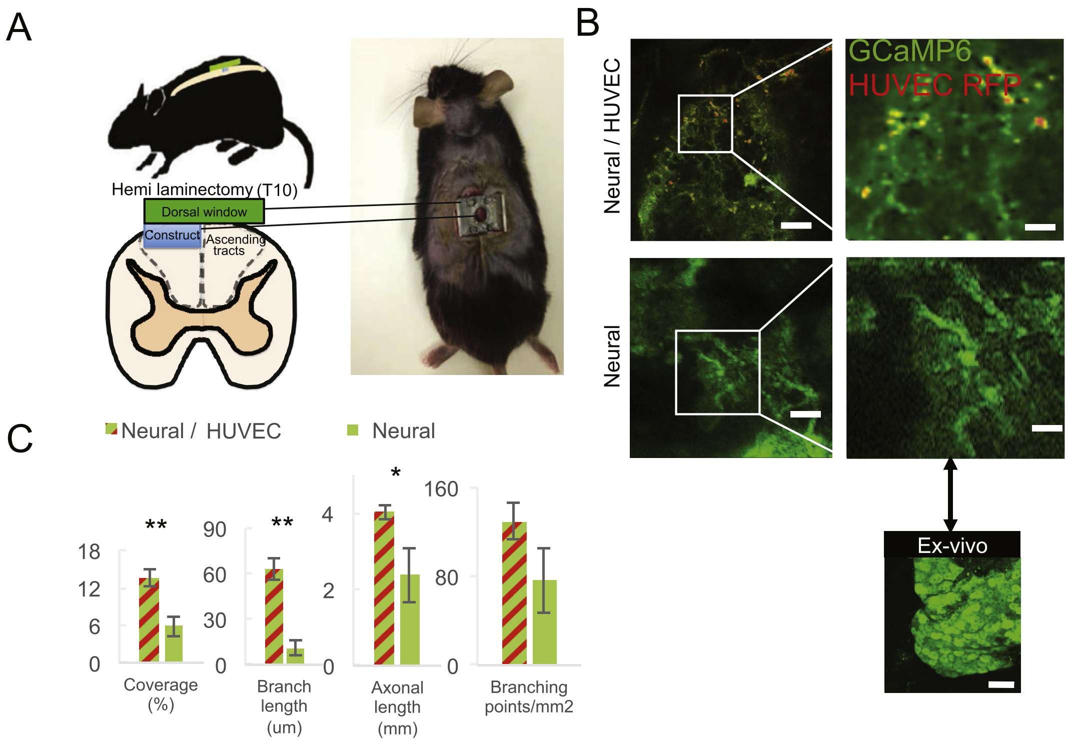


**Fig. 4. - Neuro-vascular *in vivo* implants exhibit more complex morphology.** (A) Surgical technique. After performing hemi-transection, construct is implanted in the spinal cord at T10 in a dorsal chamber allowing for 2-photon investigation. (B) representative 2-photon images of neuro-vascular (top) vs. non-vascularized constructs (bottom). Scale bar left = 100 μm. Scale bar right = 25 μm. (C) Morphology analysis of neuronal networks *in vivo* examining coverage (up), branch length, axon length and branching points. Neuro-vascular constructs n = 5, non-vascularized constructs n = 5.

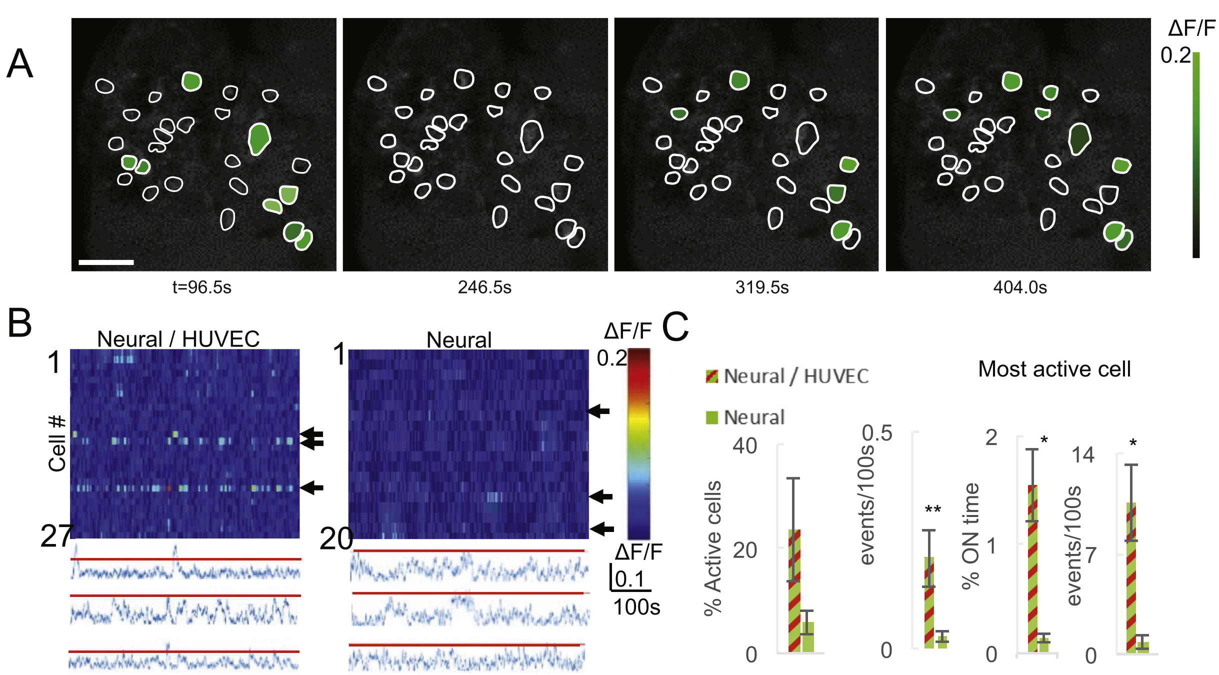


**Fig. 5. Enhanced activity is observed *in vivo* for neuro-vascular constructs.** (A) Representative epi-fluorescence neuro-vascular construct images of ΔF/F overlaid over an average intensity image, showing different neurons active at different time points. Scale bar = 30 μm. (B) Representative activity maps and representative ΔF/F temporal signals of neuro-vascular (left) vs. non-vascularized constructs (right) at day 14. Red lines indicate activity-noise threshold. (C) Activity analysis of neuro-vascular vs. non-vascularized construct characterizing % of active cells (left), total sporadic activity and the activity characteristics of the most active cell (right) at day 14. Neuro-vascular constructs n = 109 cells, 5 animals. Non-vascularized constructs n = 76 cells, 3 animals. (For interpretation of the references to colour in this figure legend, the reader is referred to the Web version of this article.)

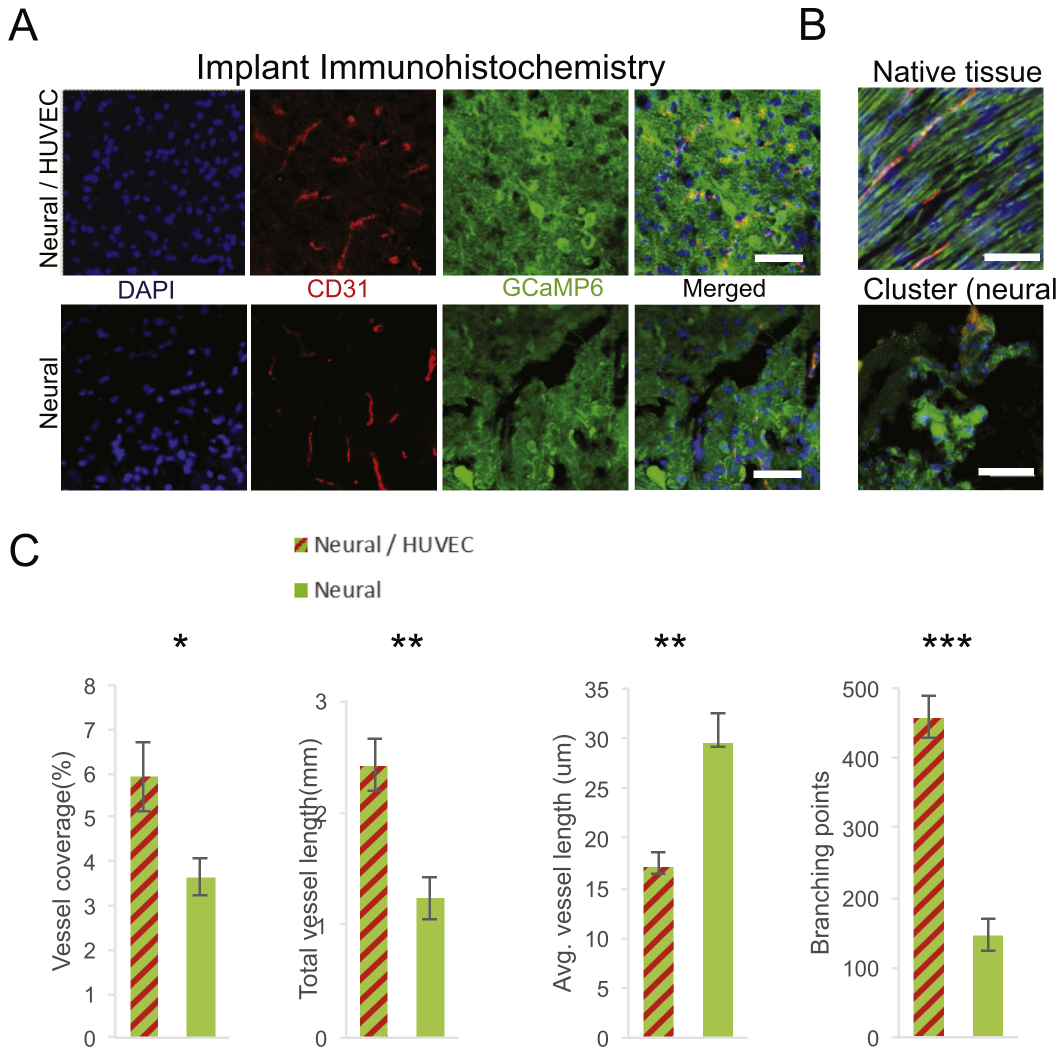


**Fig. 6. Neural-vascular constructs exhibit enhanced micro and macro-level integration.** (A) Immunohistochemistry of cryo-sections of integrated neuro-vascular implant (top) vs. non-vascularized implant (bottom). Integration of native vasculature is shown with red CD31 staining (middle). Scale bar = 30 µm. (B) Native tissue showing normal organization of axons and vasculature in the intact spinal cord (top). Cluster of neurons exhibiting "bulb" appearance in neural construct without endothelial cells (bottom). Scale bar = 30 µm. (C) Morphological analysis of vasculature in neuro-vascular constructs (n = 3) vs. the non-vascularized constructs (n = 3), examining coverage, total vessel length, average vessel branch length and number of branching points. (For interpretation of the references to colour in this figure legend, the reader is referred to the Web version of this article.)

but more branching points observed in the neuro-vascular constructs indicate that the vascular network developed in the construct is more complex.

## 4. Discussion

We developed a vascularized neural construct that enables monitoring both the morphological and, importantly, functional properties of the embedded neuronal and endothelial networks. We adopted a risk mitigation technique, and started with a permissive environment of matrigel to conceptualize the study. To make this construct clinically relevant, we then selected biocompatible degradable scaffolds made of PLLA/PLGA. An application based on this scaffold was recently used in spinal cord transection injury [9]. The selection of cells from human source also stem from its applicability to future clinical applications. We previously reported that neural and endothelial cells from a human source integrate and function in rodents in various tissue engineering paradigms [9,29,32,47], making the selection of cells from other species both functional and clinically relevant.

Interestingly, we found that beyond the improvement in viability and integration [26], these constructs also yielded multilateral effects on the performance and characteristics of the tissue. The basic benefits of vascularization were observed both in Matrigel-suspended cultures [47], and in the more readily implantable and translatable PLLA-PLGA constructs. Moreover, the findings obtained in the *in vitro* stage generally corresponded well with those in the *in vivo* environment (Fig. 4). The clusters observed in the *in vitro* studies were also abundant in mice transplanted with non-vascularized constructs. While the *in vivo* networks overall exhibited a lower structural complexity, the coverage, number of branching points and axonal length of the neuro-vascular constructs were significantly higher. Although a detailed dissection of the underlying mechanisms is deferred to future studies, some of these observed effects are likely attributed to up-regulation of secreted angiogenic and neurotrophic factors such as VEGF-A, which plays a major dual role in both vascular and neural network development [38,48,49]. For example, the over expression of NTF3 and NGFR is a probable outcome of such cellular signaling, contributing in turn to the neural proliferation exhibited by the neuro-vascular construct. The enhanced guidance cues present in the neuro-vascular constructs putatively contributed to the formation of an endothelial-neural network exhibiting wider coverage, elongated axons and featuring higher overall complexity (Figs. 1 and 2). Conversely, the clusters in the neural constructs lacking endothelial cells could result from axon outgrowth inhibition due to a lack of guidance signaling, and highly resemble dystrophic end bulbs [50] (Figs. 1C and 4B). Further, the appearance of a pronounced peak in the radial cross correlation function between the neurons and endothelial cells suggests an attraction-repulsion mechanism [38,51] that putatively leads to an 'optimal distance' of ~50 μm (Fig. 2C). This behavior likely suggests the existence of a strong interplay between the endothelial and neural cells that may also be enhancing the properties of the neuro-vascular constructs. This interplay is crucial to up regulate secretion of neurotrphic and neuroprotective factors, as this is an enabler for therapeutic solutions, possibly for dementia [52], spinal cord injury [53] and other medical conditions [54].

Does vascularization affect activity? Previous studies of vascularized cultures were focused on the formation of functional vasculature [33,34,37,55], while studies that focused on network activity used non-vascularized 3D neuronal constructs [39,56]. Here, we undertook an integrative approach that included studying the activity patterns of neural vs. neuro-vascular 3D constructs. In the permissive environment of a Matrigel we observed strong modulation of activity properties (Supplementary Fig. S3), a trend retained in the less permissive, more controllable environment of fibrin/PLLA/PLGA (Fig. 3). Both constructs exhibited a similar sporadic activity, but the concurrent network bursting activity was only pronounced in the neuro-vascular constructs, consistent with their more highly inter connected, developed morphology. Here too the basic results generalized to the *in vivo* conditions: activity signals in the neuro-vascular constructs also showed a larger fraction of viable, active cells with stronger sporadic activity and significantly higher ON time (Fig. 5).

A larger number of wider vessels were observed in the neuro-vascular constructs, and the host-specific vessel staining indicates that these constructs also led to an overall better integration into the host (Fig. 6). In particular, the host's endothelial cells penetrated the construct as indicated in the overall coverage of the construct's vasculature. Moreover, the vascular morphology was also substantially different: the neuro-vascular constructs exhibited longer overall vessels with more branches, as opposed to the neural constructs in which vessels formed but developed longer branches with lower complexity. This appears to resonate with the mechanism creating a more complex *neural* morphology in the neuro-vascular constructs: the interplay between neural and endothelial cells apparently creates complicated morphology of neural and endothelial networks altogether. Paralleling similar results in other vascularized constructs [28,30,32,57], the enhanced vascularization exhibited 7 days post-implantation indicates that the seeded endothelial cells played an important role not only in enhancing the neural activity but also in inducing the formation of a more developed vasculature.

Considering the complexity of tissue repair in various CNS disorders, our data suggests that bioengineered neuro-vascular constructs enhance neural activity and induce processes that could enhance integration and viability. Furthermore, the ability to monitor this activity both *in vitro* and *in vivo* may be a critical feature in future developments. To gain clinical relevance, the treatment design exploited an implant fabricated from FDA-approved, biocompatible and biodegradable materials, and we also note that autologous endothelial cells for vascularization can be obtained from an easily accessible source (e.g., adipose tissue). While the current construct implementation might be suitable for several conditions such as retina degeneration [58] and spinal cord injury [59], This approach shows promising preliminary results and compels further development of clinical neuronal regeneration implants inducing repair of the CNS, and study of the mechanisms underlying the observed benefits.

## Author contributions

E.S, S.S and S.L designed the experiments. E.S, U.M, I.B performed the experiments. E.S, U.M, I.B, S.S and S.L wrote and edited the manuscript.

## Conflicts of interest

The authors have no competing interests.

## Data availability

All experimental data required to reproduce the findings from this study will be made available to interested investigators.

## Acknowledgments

We thank Inbal Michael for providing technical support, Anat Marom, Erwan Poivet and Justin Little for fruitful discussions. This study was supported by the J&J Shervington Fund, Australia. Israel Foundation for Spinal Cord Injury, Israel. HOLOVISION and ENG-VASC refer to the European Research Council (ERC) grants.

## Appendix A. Supplementary data

Supplementary data related to this article can be found at https://doi.org/10.1016/j.biomaterials.2018.07.001.

## References

[1] D. Tso, R.D. McKinnon, Cell replacement therapy for central nervous system diseases, Neural Regen Res 10 (9) (2015) 1356–1358.
[2] A.R. Maldonado-Soto, D.H. Oakley, H. Wichterle, J. Stein, F.K. Doetsch, C.E. Henderson, Stem cells in the nervous system, Am. J. Phys. Med. Rehabil. 93 (11 Suppl 3) (2014) S132–S144.
[3] M.J. Glat, D. Offen, Cell and gene therapy in Alzheimer's disease, Stem Cell. Dev. 22 (10) (2013) 1490–1496.
[4] C.H. Chou, H.C. Fan, D.Y. Hueng, Potential of neural stem cell-based therapy for Parkinson's disease, Parkinsons Dis 2015 (2015) 571475.
[5] C. Benkler, D. Offen, E. Melamed, L. Kupershmidt, T. Amit, S. Mandel, M.B. Youdim, O. Weinreb, Recent advances in amyotrophic lateral sclerosis research: perspectives for personalized clinical application, EPMA J. 1 (2) (2010) 343–361.
[6] K.A. Choi, I. Hwang, H.S. Park, S.I. Oh, S. Kang, S. Hong, Stem cell therapy and cellular engineering for treatment of neuronal dysfunction in Huntington's disease, Biotechnol. J. 9 (7) (2014) 882–894.
[7] J. Drouin-Ouellet, The potential of alternate sources of cells for neural grafting in Parkinson's and Huntington's disease, Neurodegener. Dis. Manag. 4 (4) (2014) 297–307.
[8] S. David, A.J. Aguayo, Axonal elongation into peripheral nervous system "bridges" after central nervous system injury in adult rats, Science 214 (4523) (1981) 931–933.
[9] J. Ganz, E. Shor, S. Guo, A. Sheinin, I. Arie, I. Michaelevski, S. Pitaru, D. Offen, S. Levenberg, Implantation of 3D constructs embedded with oral mucosa-derived cells induces functional recovery in rats with complete spinal cord transection, Front. Neurosci. 11 (2017) 589.
[10] N.A. Silva, N. Sousa, R.L. Reis, A.J. Salgado, From basics to clinical: a comprehensive review on spinal cord injury, Prog Neurobiol 114 (2014) 25–57.
[11] C. Martínez-Ramos, U. Gómez-Pinedo, M.A. Esparza, J.M. Soria, J.A. Barcia, M. Monleón Pradas, Neural tissue regeneration in experimental brain injury model with channeled scaffolds of acrylate copolymers, Neurosci. Lett. 598 (2015) 96–101.
[12] Y. Mu, F. Wu, Y. Lu, L. Wei, W. Yuan, Progress of electrospun fibers as nerve conduits for neural tissue repair, Nanomedicine 9 (12) (2014) 1869–1883.
[13] M. Gao, P. Lu, B. Bednark, D. Lynam, J.M. Conner, J. Sakamoto, M.H. Tuszynski, Templated agarose scaffolds for the support of motor axon regeneration into sites of complete spinal cord transection, Biomaterials 34 (5) (2013) 1529–1536.

[14] T. Squillaro, G. Peluso, U. Galderisi, Clinical trials with mesenchymal stem cells: an update, Cell Transplant. 25 (5) (2016) 829–848 doi:10.3727/096368915X689622.Epub 2015 Sep 29.
[15] P. Lu, Y. Wang, L. Graham, K. McHale, M. Gao, D. Wu, J. Brock, A. Blesch, E.S. Rosenzweig, L.A. Havton, B. Zheng, J.M. Conner, M. Marsala, M.H. Tuszynski, Long-distance growth and connectivity of neural stem cells after severe spinal cord injury, Cell 150 (6) (2012) 1264–1273.
[16] J.C. Bartolomei, C.A. Greer, Olfactory ensheathing cells: bridging the gap in spinal cord injury, Neurosurgery 47 (5) (2000) 1057–1069.
[17] P. Lu, G. Woodruff, Y. Wang, L. Graham, M. Hunt, D. Wu, E. Boehle, R. Ahmad, G. Poplawski, J. Brock, L.S. Goldstein, M.H. Tuszynski, Long-distance axonal growth from human induced pluripotent stem cells after spinal cord injury, Neuron 83 (4) (2014) 789–796.
[18] P. Tabakow, W. Jarmundowicz, B. Czapiga, W. Fortuna, R. Miedzybrodzki, M. Czyz, J. Huber, D. Szarek, S. Okurowski, P. Szewczyk, A. Gorski, G. Raisman, Transplantation of autologous olfactory ensheathing cells in complete human spinal cord injury, Cell Transplant. 22 (9) (2013) 1591–1612.
[19] P. Tabakow, G. Raisman, W. Fortuna, M. Czyz, J. Huber, D. Li, P. Szewczyk, S. Okurowski, R. Miedzybrodzki, B. Czapiga, B. Salomon, A. Halon, Y. Li, J. Lipiec, A. Kulczyk, W. Jarmundowicz, Functional regeneration of supraspinal connections in a patient with transected spinal cord following transplantation of bulbar olfactory ensheathing cells with peripheral nerve bridging, Cell Transplant. 23 (12) (2014) 1631–1655.
[20] A.M. Hopkins, E. DeSimone, K. Chwalek, D.L. Kaplan, 3D in vitro modeling of the central nervous system, Prog Neurobiol 125 (2015) 1–25.
[21] D.K. Cullen, J.A. Wolf, V.N. Vernekar, J. Vukasinovic, M.C. LaPlaca, Neural tissue engineering and biohybridized microsystems for neurobiological investigation in vitro (Part 1), Crit. Rev. Biomed. Eng. 39 (3) (2011) 201–240.
[22] A. Marom, S.K. Mahto, E. Shor, J. Tenenbaum-Katan, J. Sznitman, S. Shoham, Microfluidic chip for site-specific neuropharmacological treatment and activity probing of 3D neuronal, Optonet" Cultures, Adv Healthc Mater 4 (10) (2015), 1478-83, 1422.
[23] A. Ramón-Cueto, C. Muñoz-Quiles, Clinical application of adult olfactory bulb ensheathing glia for nervous system repair, Exp. Neurol. 229 (1) (2011) 181–194.
[24] S. Levenberg, R. Langer, Advances in tissue engineering, Curr. Top. Dev. Biol. 61 (2004) 113–134.
[25] M.S. Beattie, A.A. Farooqui, J.C. Bresnahan, Review of current evidence for apoptosis after spinal cord injury, J. Neurotrauma 17 (10) (2000) 915–925.
[26] T. Kaully, K. Kaufman-Francis, A. Lesman, S. Levenberg, Vascularization—the conduit to viable engineered tissues, Tissue Eng. B Rev. 15 (2) (2009) 159–169.
[27] S. Levenberg, J. Rouwkema, M. Macdonald, E.S. Garfein, D.S. Kohane, D.C. Darland, R. Marini, C.A. van Blitterswijk, R.C. Mulligan, P.A. D'Amore, R. Langer, Engineering vascularized skeletal muscle tissue, Nat. Biotechnol. 23 (7) (2005) 879–884.
[28] J. Koffler, K. Kaufman-Francis, Y. Shandalov, S. Yulia, D. Egozi, E. Dana, D.A. Pavlov, A.P. Daria, A. Landesberg, S. Levenberg, Improved vascular organization enhances functional integration of engineered skeletal muscle grafts, Proc. Natl. Acad. Sci. U. S. A. 108 (36) (2011) 14789–14794.
[29] A. Lesman, M. Habib, O. Caspi, A. Gepstein, G. Arbel, S. Levenberg, L. Gepstein, Transplantation of a tissue-engineered human vascularized cardiac muscle, Tissue Eng. 16 (1) (2010) 115–125.
[30] A. Lesman, L. Gepstein, S. Levenberg, Cell tri-culture for cardiac vascularization, Meth. Mol. Biol. 1181 (2014) 131–137.
[31] K. Kaufman-Francis, J. Koffler, N. Weinberg, Y. Dor, S. Levenberg, Engineered vascular beds provide key signals to pancreatic hormone-producing cells, PLoS One 7 (7) (2012) e40741.
[32] Y. Shandalov, D. Egozi, J. Koffler, D. Dado-Rosenfeld, D. Ben-Shimol, A. Freiman, E. Shor, A. Kabala, S. Levenberg, An engineered muscle flap for reconstruction of large soft tissue defects, Proc. Natl. Acad. Sci. U. S. A. 111 (16) (2014) 6010–6015.
[33] M.C. Ford, J.P. Bertram, S.R. Hynes, M. Michaud, Q. Li, M. Young, S.S. Segal, J.A. Madri, E.B. Lavik, A macroporous hydrogel for the coculture of neural progenitor and endothelial cells to form functional vascular networks in vivo, Proc. Natl. Acad. Sci. U. S. A. 103 (8) (2006) 2512–2517.
[34] Q. Li, M.C. Ford, E.B. Lavik, J.A. Madri, Modeling the neurovascular niche: VEGF- and BDNF-mediated cross-talk between neural stem cells and endothelial cells: an in vitro study, J. Neurosci. Res. 84 (8) (2006) 1656–1668.
[35] H. Teng, Z.G. Zhang, L. Wang, R.L. Zhang, L. Zhang, D. Morris, S.R. Gregg, Z. Wu, A. Jiang, M. Lu, B.V. Zlokovic, M. Chopp, Coupling of angiogenesis and neurogenesis in cultured endothelial cells and neural progenitor cells after stroke, J. Cerebr. Blood Flow Metabol. 28 (4) (2008) 764–771.
[36] C.A. Jones, D.Y. Li, Common cues regulate neural and vascular patterning, Curr. Opin. Genet. Dev. 17 (4) (2007) 332–336.
[37] Y. Aizawa, M.S. Shoichet, The role of endothelial cells in the retinal stem and progenitor cell niche within a 3D engineered hydrogel matrix, Biomaterials 33 (21) (2012) 5198–5205.
[38] F. Mackenzie, C. Ruhrberg, Diverse roles for VEGF-A in the nervous system, Development 139 (8) (2012) 1371–1380.
[39] A. Marom, E. Shor, S. Levenberg, S. Shoham, Spontaneous activity characteristics of 3D "optonets, Front. Neurosci. 10 (2016) 602.
[40] M.J. Farrar, I.M. Bernstein, D.H. Schlafer, T.A. Cleland, J.R. Fetcho, C.B. Schaffer, Chronic in vivo imaging in the mouse spinal cord using an implanted chamber, Nat. Methods 9 (3) (2012) 297–302.
[41] C. Li, P. Tam, An iterative algorithm for minimum cross entropy thresholding, Pattern Recogn. Lett. 18 (8) (1998) 771–776.
[42] Ta-Chih Lee, Rangasami L. Kashyap, C.-N. Chu, Building skeleton models via 3-D medial surface/axis thinning algorithms, CVGIP Graph. Models Image Process. 56 (6) (1994) 462–478.
[43] R.Q. Quiroga, Z. Nadasdy, Y. Ben-Shaul, Unsupervised spike detection and sorting with wavelets and superparamagnetic clustering, Neural Comput. 16 (8) (2004) 1661–1687.
[44] R. Langer, J.P. Vacanti, Tissue engineering, Science 260 (5110) (1993) 920–926.
[45] T.W. Chen, T.J. Wardill, Y. Sun, S.R. Pulver, S.L. Renninger, A. Baohan, E.R. Schreiter, R.A. Kerr, M.B. Orger, V. Jayaraman, L.L. Looger, K. Svoboda, D.S. Kim, Ultrasensitive fluorescent proteins for imaging neuronal activity, Nature 499 (7458) (2013) 295–300.
[46] S. Kügler, E. Kilic, M. Bähr, Human synapsin 1 gene promoter confers highly neuron-specific long-term transgene expression from an adenoviral vector in the adult rat brain depending on the transduced area, Gene Ther. 10 (4) (2003) 337–347.
[47] A. Lesman, J. Koffler, R. Atlas, Y.J. Blinder, Z. Kam, S. Levenberg, Engineering vessel-like networks within multicellular fibrin-based constructs, Biomaterials 32 (31) (2011) 7856–7869.
[48] E. Bogaert, P. Van Damme, K. Poesen, J. Dhondt, N. Hersmus, D. Kiraly, W. Scheveneels, W. Robberecht, L. Van Den Bosch, VEGF protects motor neurons against excitotoxicity by upregulation of GluR2, Neurobiol. Aging 31 (12) (2010) 2185–2191.
[49] M.M. Nowacka, E. Obuchowicz, Vascular endothelial growth factor (VEGF) and its role in the central nervous system: a new element in the neurotrophic hypothesis of antidepressant drug action, Neuropeptides 46 (1) (2012) 1–10.
[50] S. Ramon, Y. Cajal, Degeneration & Regeneration of the Nervous System, Oxford University Press, Humphrey Milford, London, 1928.
[51] Q. Schwarz, C. Gu, H. Fujisawa, K. Sabelko, M. Gertsenstein, A. Nagy, M. Taniguchi, A.L. Kolodkin, D.D. Ginty, D.T. Shima, C. Ruhrberg, Vascular endothelial growth factor controls neuronal migration and cooperates with Sema3A to pattern distinct compartments of the facial nerve, Genes Dev. 18 (22) (2004) 2822–2834.
[52] C. Iadecola, The pathobiology of vascular dementia, Neuron 80 (4) (2013) 844–866.
[53] B. Xia, Y. Lv, Dual-delivery of VEGF and NGF by emulsion electrospun nanofibrous scaffold for peripheral nerve regeneration, Mater Sci Eng C Mater Biol Appl 82 (2018) 253–264.
[54] S. Forostyak, P. Jendelova, E. Sykova, The role of mesenchymal stromal cells in spinal cord injury, regenerative medicine and possible clinical applications, Biochimie 95 (12) (2013) 2257–2270.
[55] A.K. Achyuta, A.J. Conway, R.B. Crouse, E.C. Bannister, R.N. Lee, C.P. Katnik, A.A. Behensky, J. Cuevas, S.S. Sundaram, A modular approach to create a neurovascular unit-on-a-chip, Lab a Chip 13 (4) (2013) 542–553.
[56] H. Dana, A. Marom, S. Paluch, R. Dvorkin, I. Brosh, S. Shoham, Hybrid multiphoton volumetric functional imaging of large-scale bioengineered neuronal networks, Nat. Commun. 5 (2014) 3997.
[57] A. Freiman, Y. Shandalov, D. Rozenfeld, E. Shor, S. Segal, D. Ben-David, S. Meretzki, D. Egozi, S. Levenberg, Adipose-derived endothelial and mesenchymal stem cells enhance vascular network formation on three-dimensional constructs in vitro, Stem Cell Res. Ther. 7 (2016) 5.
[58] K. Li, X. Zhong, S. Yang, Z. Luo, Y. Liu, S. Cai, H. Gu, S. Lu, H. Zhang, Y. Wei, J. Zhuang, Y. Zhuo, Z. Fan, J. Ge, HiPSC-derived retinal ganglion cells grow dendritic arbors and functional axons on a tissue-engineered scaffold, Acta Biomater. 54 (2017) 117–127.
[59] E.Z. Yang, G.W. Zhang, J.G. Xu, S. Chen, H. Wang, L.L. Cao, B. Liang, X.F. Lian, Multichannel polymer scaffold seeded with activated Schwann cells and bone mesenchymal stem cells improves axonal regeneration and functional recovery after rat spinal cord injury, Acta Pharmacol. Sin. 38 (5) (2017) 623–637.